Radiative thermal neutron-capture cross sections for the ^{180}W(n,γ) reaction and determination of the neutron-separation energy

A. M. Hurst, R. B. Firestone, L. Szentmiklósi, B. W. Sleaford, M. S. Basunia, T. Belgya, J. E. Escher, M. Krtička, Zs. Révay, and N. C. Summers

Phys. Rev. C **92**, 034615 — Published 24 September 2015

DOI: 10.1103/PhysRevC.92.034615

Radiative thermal neutron-capture cross sections for the ^{180}W(n,γ) reaction and determination of the neutron-separation energy

A. M. Hurst,[1,*] R. B. Firestone,[1] L. Szentmiklósi,[2] B. W. Sleaford,[3] M. S. Basunia,[1]
T. Belgya,[2] J. E. Escher,[3] M. Krtička,[4] Zs. Révay,[2,5] and N. C. Summers[3]

[1] *Lawrence Berkeley National Laboratory, Berkeley, California 94720, USA*
[2] *Centre for Energy Research, Hungarian Academy of Sciences, H-1525 Budapest, Hungary*
[3] *Lawrence Livermore National Laboratory, Livermore, California 94550, USA*
[4] *Charles University in Prague, Faculty of Mathematics and Physics, CZ-180 00 Prague, Czech Republic*
[5] *Technische Universität München, Forschungsneutronenquelle Heinz Maier-Leibnitz (FRM II), Garching, Germany*

(Dated: August 28, 2015)

Prompt thermal neutron-capture partial γ-ray production cross sections were measured for the first time for the ^{180}W(n,γ) reaction using a cold guided-neutron beam at the Budapest Research Reactor. Absolute ^{181}W γ-ray cross sections were internally standardized using well-known comparator γ-ray cross sections belonging to the other tungsten isotopes present in the 11.35%-enriched ^{180}W sample. Transitions were assigned to levels in ^{181}W based largely upon information available in the literature. The total radiative thermal neutron-capture cross section σ_0 was determined from the sum of direct prompt γ-ray cross sections populating the ground state and a modeled contribution accounting for ground-state feeding from the quasi continuum. In this work, we find $\sigma_0 = 21.67(77)$ b. A new measurement of the cross section for the $5/2^-$ metastable isomer at 365.6 keV, $\sigma_{5/2^-}(^{181}\mathrm{W}^m,\ 14.6\ \mu\mathrm{s}) = 19.96(55)$ b, is also determined. Additionally, primary γ rays, observed for the first time in the ^{180}W(n,γ) reaction, provide the most precise determination for the ^{181}W neutron-separation energy, $S_n = 6669.02(16)$ keV.

PACS numbers: 28.20.Ka, 27.70.+q, 24.60.Dr, 21.10.-k

I. INTRODUCTION

The rare isotope ^{180}W, natural abundance 0.12 % [1], occupies a region of the nuclear landscape shielded by surrounding stable isotopes from r-process β^--decay chains, and is also outside the path of the s-process. Both the rapid (r) and slow (s) neutron-capture processes play crucial roles for the nucleosynthesis of heavy elements and the evolution of stars, with additional processes, for example, the secondary p-process, relevant for explaining specific abundance patterns. Indeed, ^{180}W is expected to be formed in the γ aspect of the p-process through a successive series of photodisintegration (γ,n) reactions from s-process seeds during shockwave passage in the neon-oxygen shells in Type II supernovae [2, 3]. As the most proton-rich stable isotope of tungsten, it is an important isotope as it is expected to control the abundances of lighter p-nuclei, in particular ^{174}Hf. Given that there are only 32 stable nuclei available for p-process studies [2], experimental data for these nuclei are critical to develop our understanding of mechanisms underlying this process. Also, due to the scarcity of p-process nuclei in nature (always the least abundant in an isotopic chain [2]), for certain isotopes, precise physical properties remain elusive or debatable in the context of the current literature. Consequently, new measurements are needed to improve or verify the quality of data for p-process nuclei. New measurements can also have fundamental implications for nuclear structure and reaction physics.

In this paper we revisit the total radiative-capture cross section (σ_0) for ^{180}W(n,γ) using thermal neutrons. Hitherto, there exists only sparse information regarding σ_0 for ^{180}W(n,γ) and there is considerable scatter amongst the published literature values: 30^{+120}_{-30} b [4]; 22.6±1.7 b [5]; and 37.3±2.4 b [6]. Therefore, new measurements of σ_0 are needed to determine the reliability of previous results. In addition, we have measured the neutron separation energy (S_n) for the ^{181}W compound, from the analysis of primary γ rays (i.e. those originating at S_n) to low-lying states following neutron capture on ^{180}W. The present adopted value for $S_n(^{181}\mathrm{W})$ is poorly known at 6686(5) keV [7]. Improved accuracy and precision in S_n is clearly desirable for this nucleus and such improvements will provide new data for future atomic mass evaluations.

This work also represents the most complete spectroscopic study of ^{181}W from radiative neutron capture. The partial γ-ray production cross sections (σ_γ) deduced in this analysis, together with σ_0, provide essential data for the augmentation of other neutron data libraries, such as the Evaluated Nuclear Data File (ENDF) [8] and the Reference Input Parameter Library (RIPL) [9], which are used in a variety of modeling applications. The thermal cross sections reported in this work are particularly relevant for several areas of societal importance, including: addressing the fallout activity from ^{181}W in thermonuclear-weapons testing [10–12]; the potential use for ^{181}W as a medical isotope in the treatment of brachytherapy [13]; fusion and accelerator-driven reactor designs based on neutron targets comprising natural

*Electronic address: AMHurst@lbl.gov

TABLE I: Select partial γ-ray production cross sections corresponding to (n,γ) reactions on the major tungsten isotopes. The data are taken from Ref. [20]. The last column lists the results of the current measurement campaign.

Target	E_γ [keV]	σ_γ [b] [a]	σ_γ [b] [b]	σ_γ [b] [c]
^{182}W [d]	98.9	0.342(12)	0.146(5)	0.145(4)
^{182}W [d]	162.1	0.9834(27)	0.4209(12)	0.414(14)
^{182}W [d]	291.6	0.2510(93)	0.1074(40)	0.1093(37)
^{182}W	1100.4	0.127(27)	0.054(11)	0.0582(32)
^{182}W [d]	6190.8	2.740(38)	1.173(16)	1.151(33)
^{183}W	111.2	1.600(44)	0.2363(65)	0.2565(80)
^{183}W	215.3	0.0959(51)	0.01419(76)	0.0121(9)
^{183}W	792.1	1.157(50)	0.1712(74)	0.1544(58)
^{184}W	173.7	0.0679(48)	0.01344(95)	0.0129(15)
^{186}W [d]	145.8	4.727(46)	0.5328(52)	0.534(16)
^{186}W [d]	273.1	1.337(14)	0.1506(16)	0.1540(46)
^{186}W	1082.2	0.309(17)	0.0348(19)	0.0404(20)

[a] Absolute partial γ-ray production cross sections assuming 100% enrichment; taken from Ref. [20].

[b] Calculated partial γ-ray production cross sections assuming the isotopic abundances of the 11.35%-enriched ^{180}W sample: ^{182}W 42.80%, ^{183}W 14.80%, ^{184}W 19.80%, and ^{186}W 11.27%.

[c] Partial γ-ray production cross sections deduced in this work for the 11.35%-enriched ^{180}W sample.

[d] Transition used for ^{180}W(n,γ) normalization.

tungsten where ^{181}W represents a major contaminant activity [14–17]. Furthermore, ^{180}W has been identified as a candidate progenitor for an artificial neutrino source (with ^{181}W the β^--decaying radioactive product) which could be used in the calibration of neutrino detectors [18, 19] as well as for studying fundamental properties of the neutrino itself. In this case, a reliable measurement of σ_0 (in addition to other properties outlined in Ref. [5]) is needed to assess its suitability.

II. EXPERIMENT AND DATA ANALYSIS

Partial γ-ray production cross sections (σ_γ) for the ^{180}W(n,γ) reaction were measured using the cold-neutron source at the 10-MW Budapest Research Reactor [21, 22]. This measurement exploited the prompt-γ decay of the corresponding ^{181}W compound nucleus utilizing a 4-mg sample of an 11.35% enriched ^{180}W oxide powder at the Prompt Gamma Activation Analysis (PGAA) facility [23, 24]. Contaminant tungsten isotopes were present in the sample with abundances: ^{182}W 42.80%; ^{183}W 14.80%; ^{184}W 19.80%; and ^{186}W 11.27%. The spectrographic-assay analysis reveals negligible amounts of trace-element impurities in the sample ($<$ 500 ppm). The PGAA setup is located approximately 33.5 m downstream of the reactor at the end of a slightly curved guide coated with $2\theta_c$ supermirror elements [25]. The guide is comprised of borofloat glass with a modular aluminium flight tube at the end. The flight tube is lined with a ^{6}Li-doped polymer to decrease neutron scatter. An intense neutron flux of 7.75×10^7 n·cm^{-2}·s^{-1}, with an equivalent neutron temperature distributed around $T\approx140$ K [26, 27], is achieved at the target position of the PGAA sample chamber. The PGAA facility comprises an n-type coaxial High-Purity Germanium (HPGe) detector with an active volume of 144 cm^3 and a relative efficiency of 27% at 1332 keV. The HPGe detector is surrounded by an eight-segment coaxial bismuth germanate (BGO) Compton-suppression shield, and together, this system is mounted inside a 10-cm thick lead container which is also coated with a ^{6}Li-containing plastic layer for γ-ray absorption and neutron shielding, respectively. The adopted shielding provides a very low background-radiation level of around 10-20 counts/s with the neutron beam on (falling to $\sim$ 0.9 counts/s with no beam) [28]. There is no contribution from epithermal or fast neutrons. The sample-to-detector distance is 23.5 cm which minimizes peak-summing effects [23]. The enriched ^{180}W oxide powder was placed inside a Teflon bag (transparent to neutrons and γ rays to a reasonable approximation) and placed in the sample holder at an angle of 30° relative to the beam direction during neutron bombardment. Prompt γ-ray data were collected for a 64.6-h period and the corresponding singles energy spectra were analyzed offline using the HYPERMET-PC analysis software package [24, 29–32]. Representative prompt γ-ray spectra corresponding to the irradiated 11.35% ^{180}W enriched sample are presented in Fig. 1.

Transitions from contaminant tungsten isotopes are clearly apparent in the measurement with the enriched-^{180}W sample. Therefore, unknown partial γ-ray production cross sections (σ_{γ_u}) for transitions from ^{180}W(n,γ) may be deduced relative to the known comparator absolute cross sections (σ_{γ_s}) from the other tungsten isotopes [20] by adopting an internal-standardization procedure similar to that described in Ref. [33]. In general, transition cross sections may be extracted from their measured peak areas (A_γ) according to the expression

$$A_\gamma = \frac{mN_A}{M}\theta\sigma_\gamma\epsilon_\gamma(E_\gamma)f(E_\gamma)\phi T, \tag{1}$$

where, m is the sample mass, M is the relative atomic mass, N_A is the Avogadro number, θ is the isotopic abundance, $\epsilon_\gamma(E_\gamma)$ denotes the relative E_γ-dependent detection efficiency [31, 34], $f(E_\gamma)$ is the E_γ-dependent self-attenuation correction factor for neutron self shielding and γ-ray absorption [26, 35], ϕ is the neutron flux, and T represents the deadtime-corrected irradiation period. Because the standardization approach is a relative measurement, many systematic errors (m, M, N_A, ϕ, and T) are eliminated using the following relation

$$\frac{A_{\gamma_u}}{A_{\gamma_s}} = \frac{\theta_u}{\theta_s}\cdot\frac{\epsilon_{\gamma_u}(E_\gamma)}{\epsilon_{\gamma_s}(E_\gamma)}\cdot\frac{f_u(E_\gamma)}{f_s(E_\gamma)}\cdot\frac{\sigma_{\gamma_u}}{\sigma_{\gamma_s}}. \tag{2}$$

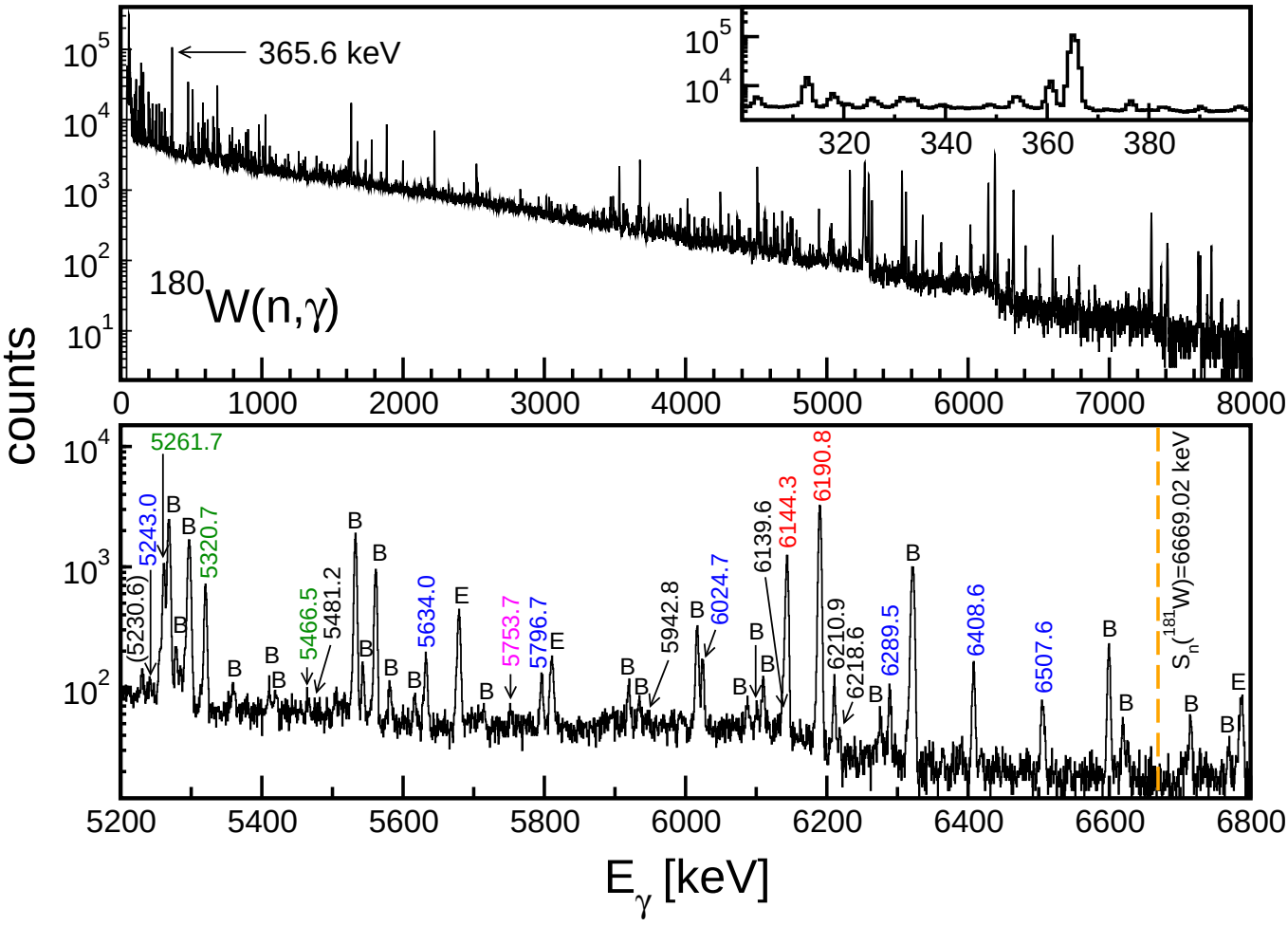

FIG. 1: (Color online) Representative prompt γ-ray spectra observed following the (n,γ) measurement using a WO_2 powder enriched to 11.35% in ^{180}W. The upper panel shows the complete energy range of interest in this measurement; the inset is expanded around $E_\gamma = 300 - 400$ keV revealing the strongest transition observed in the ^{180}W$(n,\gamma)^{181}$W reaction. A subset of characteristic primary γ rays corresponding to all naturally-occurring tungsten isotopes are labeled on the spectrum expanded around $E_\gamma = 5200 - 6600$ keV in the lower panel: ^{180}W(n,γ) black; ^{182}W(n,γ) red; ^{183}W(n,γ) blue; ^{184}W(n,γ) magenta; ^{186}W(n,γ) green. Several prominent background lines (B) and escape peaks (E) are also labeled; a dashed-orange line is drawn to indicate the lack of any transition at the expected position of the neutron-separation energy in ^{181}W (see Sect. IV C).

The subscripts u and s denote transitions in ^{181}W and comparator standards in the other tungsten isotopes, respectively. Although the WO_2 target material has a relatively high density ($\rho = 10.8$ g/cm^3), the very small amount of sample irradiated ensured that γ-ray self absorption [35] was negligible at all energies i.e. $f(E_{\gamma_u})/f(E_{\gamma_s}) \approx 1$. Previous experimental investigations adopting similar procedures are described elsewhere [20, 36–40].

A subset of strong clean transitions from the other tungsten isotopes observed in this work are listed in Table I. Their cross sections are taken from Ref. [20]. Transitions used for normalization of the ^{180}W$(n,\gamma)^{181}$W data to scale measured transition intensities to cross sections are indicated in the table. However, because partial γ-ray production cross sections have never before been measured for ^{180}W(n,γ), cross sections for well-resolved intense transitions observed from (n,γ) reactions on other tungsten isotopes present in the sample (i.e. transitions belonging to ^{183,184,185,187}W compounds) were also used to validate the procedure. Table I shows the expected cross sections for select transitions in these isotopes, based on their previously measured absolute cross sections (third column) [20], corrected for abundance in the irradiated sample (fourth column), together with the normalized cross sections based on the standardization procedure adopted in this study (fifth column). For all ^{182,184,186}W(n,γ) transitions the measured cross sections compare well with their expected values as shown in the final two columns of Table I. Consistency is somewhat worse for the ^{183}W(n,γ) transitions (although agreement within two standard deviations is still achieved) as the strong 111.2 and 792.1-keV transitions are partly obscured by other γ rays and rela-

tively weak in the enriched-^{180}W(n,γ) spectrum when compared to the ^{183}W(n,γ) enriched-isotope spectrum [20]. The 215.3-keV transition is also much weaker in ^{180}W(n,γ) enriched-isotope spectrum. However, overall consistency is observed for the tungsten cross sections in Table I and this also serves as an independent verification of the reported target-isotopic abundances from the spectrographic-assay analysis of the sample.

III. STATISTICAL MODEL SIMULATIONS

The total radiative thermal neutron-capture cross section (σ_0) of ^{180}W can be determined from the sum of measured partial γ-ray cross sections corresponding to transitions to the ground state of ^{181}W ($\sigma_\gamma^{\rm exp}$). In reality, σ_0 must be corrected for the intensity of the unobserved fractional contribution P_0 feeding the ground state from the *quasi continuum* which may be estimated from statistical-model calculations. The total cross section is then given by

$$\sigma_0 = \frac{\sum_{i=1}^{n} \sigma_{\gamma_i}^{\rm exp}(1+\alpha_i)}{1-P_0}, \qquad (3)$$

where the summation goes over all σ_γ feeding the ground state directly and α is an internal conversion coefficient. The fraction P_0 was obtained with the Monte Carlo program DICEBOX [41] together with other statistical γ-decay related quantities including the populations of individual low-lying levels P_L and the mean capture-state total radiative width Γ_0.

The DICEBOX algorithm is predicated on the extreme statistical model of compound nucleus formation and decay, proposed by Bohr [42], where it is assumed that microscopic nuclear structure effects can be neglected. In this theoretical framework, DICEBOX exploits experimentally-known level energies, spins, parities, and branching ratios, to describe γ decay below a certain *critical* energy, $E_{\rm c}$. It is assumed that the decay-scheme information is both accurate and complete below $E_{\rm c}$. Above $E_{\rm c}$, in the quasi continuum, levels are randomly generated from a Poisson distribution according to an *a priori* assumed level density (LD) model. Intensities of transitions between any pair of initial (E_i) and final (E_f) states, which can be characterized by a partial radiation width $\Gamma_{i\gamma f}$, originating from levels at $E_i > E_{\rm c}$ are then generated according to an *a priori* assumed photon strength function (PSF), f^{XL}, where X denotes the transition type (electric $X = E$ or magnetic $X = M$) and L represents the multipole order:

$$\Gamma_{i\gamma f} = \sum_{XL} \xi_{XL}^2 \frac{f^{XL}(1+\alpha_{XL})E_\gamma^{2L+1}}{\rho(E_i,J_i,\pi_i)}. \qquad (4)$$

Here, $\rho(E_i,J_i,\pi_i)$ is the LD for levels with spin J_i and parity π_i at an excitation energy E_i, α is the electron internal conversion coefficient obtained from the Band-Raman prescription implemented into the BRICC code [43], and ξ is a random variable drawn from a normal distribution with zero mean and unit variance, i.e. $\xi \in \mathcal{N}(0,1)$; the calculated widths thus follow a Porter-Thomas distribution [44] because the expectation value $\langle\xi\rangle = 1$. The sum in Eq. 4 goes over all transition types and multipolarities allowed by spin-parity selection rules. In practice, and in order of decay-mode dominance, only electric dipole ($E1$), magnetic dipole ($M1$), and electric quadrupole ($E2$) transitions were considered in the simulations. Individual $\Gamma_{i\gamma f}$ decay amplitudes demonstrate negligible interference and are assumed to be independent and uncorrelated.

To calculate the complete system of partial-radiation widths (Eq. 4), several combinations of PSF and LD models were adopted in the simulations. Specifically, the Constant Temperature Formula (CTF) [45] and Back-Shifted Fermi Gas (BSFG) [46] models, utilizing parametrizations from von Egidy and Bucurescu [47–49], were used for the LD. A parity dependence based on a Fermi-Dirac distribution parametrized according to the semi-empirical mass model outlined in Ref. [50] was also considered in the overall LD calculation. Introduction of the parity dependence did not influence the results, similarly for earlier investigations [20]. For the $E1$ PSF we tested the standard-Lorentzian Brink-Axel (BA) model [51, 52], the Kadmensky-Markushev-Furman (KMF) [53], the Generalized Lorentzian (GLO) [54], and the Enhanced Generalized Lorentzian (EGLO) [55]; the enhancement factor $k_0 = 3.5$ was used for the EGLO in accordance with Ref. [20]. The giant electric dipole parameters were taken from those used in earlier investigations of the tungsten isotopes [20]. Models for the $M1$ and $E2$ PSFs were also the same as those used in Ref. [20], i.e. the neutron single-particle (SP) model for the $M1$ PSF [56] with $f_{SP}^{(M1)} = 1\times10^{-9}$ MeV^{-3} and an isovector-isoscalar model for the $E2$ PSF based on a global parametrization to describe the giant electric quadrupole resonance [57, 58].

Due to the statistical fluctuations involved in the generation of individual levels and intensities of transitions there can be an infinite number of different decay schemes, even for a single PSF and LD model combination. DICEBOX calculates capture-state γ-decay cascades originating at S_n and the corresponding decay-scheme simulation is referred to as a *nuclear realization*. The random nature of the decay widths and level spacings are incorporated into each nuclear realization using a deterministic sequence of generator seeds to simulate the decay process. Because of the random decay paths

TABLE II: Experimental neutron-capture partial γ-ray production cross sections from the ^{180}W(n,γ) reaction with thermal neutrons. All spins, J, parities, π, and mixing ratios, δ_γ, are taken from the ENSDF adopted levels for ^{181}W [59] unless stated otherwise. Multipolarities, XL, in square brackets were assumed based on ΔJ angular-momentum selection rules; other values were taken from ENSDF. Assumed multipolarities from ENSDF are noted with an asterisk. The internal conversion coefficients, α, were calculated with BRICC [43]. Quantities in parentheses represent tentative assignments. Transitions in bold ($n = 13$) represent transitions to the ground state and are used for the determination of σ_0 in Eq. 3; transitions in italics ($n = 17$) feed the $5/2^-$ isomer at 365.6 keV and are used for the determination of $\sigma_{5/2^-}$ (see text for details).

E_i (keV)	$J_i^{\pi_i}$	E_f (keV)	$J_f^{\pi_f}$	E_γ (keV)	$\sigma_\gamma^{\rm exp}$ (b)	α	XL	δ_γ
0	$9/2^+$							
113.47(6)	$11/2^+$	0	$9/2^+$	**113.49(6)**	**0.144(16)**	**3.304**	$M1$	
365.56(4)	$5/2^-$	113.47(6)	$11/2^+$	252.2(3)[a]	0.227(54)	0.8159	$E3$	
		0	$9/2^+$	**365.60(4)**	**13.39(37)**	**0.4598**	$M2$	
385.26(8)	$1/2^-$	365.56(4)	$5/2^-$	*19.7(2)*[b]	*0.00174(26)*	*8329*	$E2$	
409.20(9)	$7/2^-$	365.56(4)	$5/2^-$	*43.5(2)*[c]	*0.038(18)*	*10.768*	$M1+E2$	0.10(3)
		0	$9/2^+$	**409.14(36)**	**0.0203(88)**	**0.01107**	$[E1]$	
450.23(11)	$3/2^-$	385.26(8)	$1/2^-$	65.0(2)[d]	0.96(23)	4.851	$M1+E2$	0.33(4)
457.95(9)	$1/2^-$	385.26(8)	$1/2^-$	72.68(5)[d]	0.30(11)	11.82	$[M1]$	
475.51(5)	$7/2^-$	365.56(4)	$5/2^-$	*109.91(5)*[e]	*0.265(65)*	*3.504*	$M1+E2$	0.38(7)
		0	$9/2^+$	**475.48(14)**[a]	**0.042(13)**	**0.00792**	$[E1]$	
488.42(10)	$5/2^-$	450.23(11)	$3/2^-$	38.1(2)[a]	0.052(19)	13.64	$M1$	
		385.26(8)	$1/2^-$	103.08(8)[e]	0.148(41)	3.462	$E2$	
528.72(18)	$9/2^-$	409.20(9)	$7/2^-$	119.57(16)	0.0314(51)	2.853	$[M1]*$	
529.56(10)	$3/2^-$	457.95(9)	$1/2^-$	71.7(2)[a]	0.066(29)	12.519	$M1+E2$	$0.29\binom{+6}{-4}$
		385.26(8)	$1/2^-$	144.47(13)[e]	0.219(42)	1.662	$M1$	
		365.56(4)	$5/2^-$	*163.9(2)*[a]	*0.075(33)*	*0.949*	$M1+E2$	0.8
560.56(9)	$5/2^-$	529.56(10)	$3/2^-$	31.2(2)[a]	0.0029(12)	24.86	$M1$	
		457.95(9)	$1/2^-$	102.7(2)[a]	0.044(21)	3.513	$E2$	
		450.23(11)	$3/2^-$	110.3(2)[a]	0.162(52)	3.559	$M1+E2$	0.17(7)
		385.26(8)	$1/2^-$	175.31(7)[e]	0.075(17)	0.4835	$E2$	
		365.56(4)	$5/2^-$	*195.0(2)*[a]	*0.027(12)*	*0.7154*	$M1$	
609.1(4)	$9/2^-$	475.51(5)	$7/2^-$	133.7(5)[d]	0.00943(53)	2.070	$[M1]*$	
		365.56(4)	$5/2^-$	*243.5(5)*[d]	*0.0471(26)*	*0.1619*	$[E2]$	
643.25(10)	$7/2^-$	488.42(10)	$5/2^-$	154.58(19)	0.0617(97)	0.7536	$E2$	
		475.51(5)	$7/2^-$	167.2(2)[a]	0.0222(77)	1.100	$[M1]*$	
		450.23(11)	$3/2^-$	193.2(2)[a]	0.0191(74)	0.3464	$[E2]*$	

continued on next page

[a] Multiplet resolved using ENSDF [59] branching ratios.
[b] Transition not observed; intensity estimated based on statistical-model calculations.
[c] Transition not observed; intensity deduced based on ENSDF [59] branching ratios.
[d] Multiplet resolved based on statistical-model calculations.
[e] Contaminant subtracted from multiplet based on known cross sections.
[f] Newly identified γ-ray transition based on experimental observation.
[g] Limit estimated from observed intensity feeding level.
[h] Tentative transition (see Sect. IV C); not used in fit to E_γ data.
[i] Weak transition; not used in fit to E_γ data.

TABLE II: *continued*

E_i (keV)	$J_i^{\pi_i}$	E_f (keV)	$J_f^{\pi_f}$	E_γ (keV)	$\sigma_\gamma^{\exp}$ (b)	α	XL	δ_γ
		365.56(4)	$5/2^-$	*278.49(17)*[a]	*0.038(13)*	*0.2682*	$[M1]*$	
661.71(5)	$7/2^-$	475.51(5)	$7/2^-$	186.2(2)[a]	0.0364(68)	0.3928	$E2$	
		365.56(4)	$5/2^-$	*296.1(3)*[a]	*0.059(15)*	*0.173*	$M1+E2$	0.8
		0	$9/2^+$	**661.66(5)**[e]	**0.638(41)**	**0.00396**	$E1$	
674.81(16)	$11/2^-$	528.72(18)	$9/2^-$	146.6(5)[a]	0.0399(87)	1.594	$[M1]$	
		409.20(9)	$7/2^-$	265.57(14)	0.0518(85)	0.1232	$[E2]$	
714.64(12)	$7/2^-$	365.56(4)	$5/2^-$	349.06(11)[f]	0.731(88)	0.1458	$[M1]$	
726.55(5)	$3/2^-$	560.56(9)	$5/2^-$	165.8(2)[a]	0.0066(33)	0.917	$M1+E2$	0.8
		529.56(10)	$3/2^-$	197.0(2)[a]	0.028(12)	0.6953	$M1$	
		488.42(10)	$5/2^-$	237.4(3)[a]	0.0054(17)	0.4150	$[M1]*$	
		450.23(11)	$3/2^-$	276.4(3)[a]	0.0352(88)	0.209	$M1+E2$	$0.8\binom{+9}{-6}$
		409.20(9)	$7/2^-$	316.7(3)[a]	0.0049(17)	0.07239	$[E2]*$	
		385.26(8)	$1/2^-$	340.8(3)[a]	0.00211(79)	0.1555	$[M1]*$	
		365.56(4)	$5/2^-$	*361.03(4)*	*1.094(33)*	*0.078*	$M1+E2$	1.4(2)
805.5(3)	$(9/2^-)$	661.71(5)	$7/2^-$	143.1(5)	≥ 0.079[g]	1.707	$[M1]*$	
807.37(5)	$5/2^-$	643.25(10)	$7/2^-$	164.6(2)	0.024(11)	0.936	$M1+E2$	0.8
		475.51(5)	$7/2^-$	331.86(6)	0.260(14)	0.1670	$M1$	
		409.20(9)	$7/2^-$	398.20(9)	0.1048(97)	0.1027	$M1$	
		365.56(4)	$5/2^-$	*441.84(7)*	*0.228(16)*	*0.07804*	$(M1)$	
953.20(5)	$7/2^+$	113.47(6)	$11/2^+$	840.4(4)[a]	0.034(13)	0.00644	$E2$	
		0	$9/2^+$	**953.18(5)**	**0.430(25)**	**0.01090**	$M1$	
1009.45(6)	$(5/2^+, 7/2^+)$	475.51(5)	$7/2^-$	533.3(3)	0.0087(48)	0.00618	$[E1]$	
		365.56(4)	$5/2^-$	*643.9(4)*	*0.084(28)*	*0.00418*	$[E1]$	
		0	$9/2^+$	**1009.47(6)**	**0.362(78)**	**0.00944**	$[M1]$	
1086.17(6)	$(7/2^+)$	113.47(6)	$11/2^+$	973.2(4)[a]	0.0203(79)	0.00476	$[E2]$	
		0	$9/2^+$	**1086.13(6)**	**0.084(19)**	**0.00382**	$E2$	
1188.38(14)	$3/2^-$	560.56(9)	$5/2^-$	628.8(4)[a]	0.033(11)	0.03122	$[M1]*$	
		529.56(10)	$3/2^-$	659.08(33)[a]	0.059(19)	0.02768	$[M1]*$	
		488.42(10)	$5/2^-$	699.9(4)[a]	0.033(11)	0.02375	$[M1]*$	
		457.95(9)	$1/2^-$	730.1(4)[a]	0.0186(76)	0.02133	$[M1]*$	
		450.23(11)	$3/2^-$	738.0(4)[a]	0.074(26)	0.02075	$M1$	
		385.26(8)	$1/2^-$	803.6(4)[e]	0.371(30)	0.01190	$M1+E2$	1
		365.56(4)	$5/2^-$	*822.7(4)*[a]	*0.041(15)*	*0.01577*	$M1$	
1249.06(7)	$5/2^-$	1009.45(6)	$(5/2^+, 7/2^+)$	239.3(3)[a]	0.0291(88)	0.03984	$[E1]*$	
		807.37(5)	$5/2^-$	441.84(7)	0.228(16)	0.07804	$(M1)$	
		726.55(5)	$3/2^-$	522.1(3)[a]	0.073(26)	0.05045	$M1$	
		661.71(5)	$7/2^-$	587.22(8)	0.221(20)	0.01423	$E2$	
		475.51(5)	$7/2^-$	773.4(4)[a]	0.0247(88)	0.01843	$[M1]*$	
		365.56(4)	$5/2^-$	883.2(4)[a]	0.084(30)	0.01319	$M1$	

continued on next page

TABLE II: *continued*

E_i (keV)	$J_i^{\pi_i}$	E_f (keV)	$J_f^{\pi_f}$	E_γ (keV)	$\sigma_\gamma^{\rm exp}$ (b)	α	XL	δ_γ
1272.01(13)	$5/2^+$	1009.45(6)	$(5/2^+, 7/2^+)$	262.6(3)[a]	0.0238(97)	0.23102	$M1+E2$	$0.9\binom{+7}{-4}$
		953.20(5)	$7/2^+$	318.6(3)[e]	0.125(23)	0.1863	$M1$	
		409.20(9)	$7/2^-$	862.7(4)[a]	0.0200(72)	0.00235	$[E1]$	
		0	$9/2^+$	**1272.46(27)**[a]	**0.0125(44)**	**0.00282**	$[E2]$	
1330.08(14)	$(5/2^-, 7/2^-)$	805.5(3)	$(9/2^-)$	524.4(3)[a]	0.204(87)	0.04988	$[M1]*$	
		661.71(5)	$7/2^-$	668.2(4)[a]	0.33(14)	0.02673	$[M1]*$	
		560.56(9)	$5/2^-$	769.61(14)[e]	0.165(42)	0.01866	$M1$	
		475.51(5)	$7/2^-$	854.4(4)[a]	0.197(80)	0.01434	$M1$	
1355.3(3)	$(5/2^-, 7/2^-)$	661.71(5)	$7/2^-$	693.9(4)[a]	0.039(13)	0.01420	$M1+E2$	1.5
		365.56(4)	$5/2^-$	989.4(4)[e]	0.139(19)	0.00993	$M1$	
1365.57(9)	$3/2^+$	1272.01(13)	$5/2^+$	93.7(2)[a]	0.0036(16)	5.64190	$M1+E2$	$0.38\binom{+7}{-6}$
		1188.38(14)	$3/2^-$	177.5(2)[a]	0.050(22)	0.08494	$E1$	
		1009.45(6)	$(5/2^+, 7/2^+)$	356.1(3)[a]	0.052(28)	0.05165	$[E2]*$	
		953.20(5)	$7/2^+$	412.3(3)[a]	0.032(11)	0.03453	$[E2]*$	
		807.37(5)	$5/2^-$	557.8(3)[a]	0.066(19)	0.00562	$E1$	
		726.55(5)	$3/2^-$	639.0(4)[e]	0.200(40)	0.00424	$E1$	
		560.56(9)	$5/2^-$	805.2(4)[a]	0.096(52)	0.00268	$[E1]$	
		529.56(10)	$3/2^-$	835.7(4)[a]	0.0142(44)	0.00250	$[E1]$	
		488.42(10)	$5/2^-$	877.2(4)[a]	0.0140(66)	0.00228	$[E1]$	
		457.95(9)	$1/2^-$	907.4(4)[a]	0.032(11)	0.00214	$E1$	
		385.26(8)	$1/2^-$	980.7(4)[a]	0.0058(21)	0.00185	$[E1]$	
		365.56(4)	$5/2^-$	*999.87(15)*[a]	*0.091(14)*	*0.00179*	$E1$	
1377.83(14)	$(3/2^+, 5/2^+)$	807.37(5)	$5/2^-$	570.1(3)[a]	0.081(33)	0.00537	$[E1]$	
		726.56(5)	$3/2^-$	651.28(18)[e]	0.183(58)	0.00408	$E1$	
		560.56(9)	$5/2^-$	817.5(4)[a]	0.024(11)	0.00261	$[E1]$	
		529.56(10)	$3/2^-$	848.5(4)[a]	0.024(11)	0.00243	$[E1]$	
		488.42(10)	$5/2^-$	889.5(4)[a]	0.0202(74)	0.00222	$[E1]$	
1422.87(25)	$(5/2^-, 7/2^-)$	726.56(5)	$3/2^-$	696.9(4)[a]	0.138(70)	0.02401	$[M1]$	
		475.51(5)	$7/2^-$	946.9(4)[a]	0.52(18)	0.01108	$[M1]$	
		365.56(4)	$5/2^-$	*1057.1(5)*[e]	*0.693(35)*	*0.00842*	$[M1]$	
1440.11(15)	$(5/2^+, 7/2^+)$	1086.17(6)	$(7/2^+)$	353.6(3)[a]	0.02978(70)	0.1409	$(M1)$	
		953.20(5)	$7/2^+$	487.1(3)[a]	0.049(27)	0.06045	$M1$	
		807.37(5)	$5/2^-$	632.7(4)[a]	0.0104(47)	0.00433	$[E1]$	
		475.51(5)	$7/2^-$	965.1(4)[a]	0.0143(52)	0.00191	$[E1]$	
		365.56(4)	$5/2^-$	*1075.6(5)*[a]	*0.070(26)*	*0.00156*	$E1$	
		0	$9/2^+$	**1439.56(32)**	**0.130(32)**	**0.00227**	$E2$	
1468.87(16)	$(5/2^+)$	1086.17(6)	$(7/2^+)$	382.3(3)[a]	0.0122(76)	0.08630	$M1+E2$	0.8
		953.20(5)	$7/2^+$	515.7(3)[a]	0.0074(45)	0.0521	$M1$	
		475.51(5)	$7/2^-$	993.7(4)[a]	0.0096(70)	0.00181	$[E1]$	

continued on next page

TABLE II: *continued*

E_i (keV)	$J_i^{\pi_i}$	E_f (keV)	$J_f^{\pi_f}$	E_γ (keV)	$\sigma_\gamma^{\rm exp}$ (b)	α	XL	δ_γ
		450.23(11)	$3/2^-$	1018.6(5)[a]	0.0059(36)	0.00173	[$E1$]	
		365.56(4)	$5/2^-$	*1103.5(5)*[a]	*0.032(19)*	*0.00150*	$E1$	
		0	$9/2^+$	**1469.2(5)**	**0.037(19)**	**0.00219**	$E2$	
1498.12(18)	$(5/2)^+$	1009.45(6)	$(5/2^+, 7/2^+)$	489.0(3)[e]	0.110(19)	0.05983	$M1$	
		953.20(5)	$7/2^+$	544.8(3)[a]	0.043(16)	0.04518	[$M1$]	
		365.56(4)	$5/2^-$	*1132.3(5)*[a]	*0.033(12)*	*0.00143*	[$E1$]	
		113.47(6)	$11/2^+$	1384.2(5)[a]	0.034(12)	0.00243	$E2$	
		0	$9/2^+$	**1498.2(5)**[a]	0.0122(48)	**0.00213**	[$E2$]	
1537.3(4)	$(7/2^+)$	0	$9/2^+$	**1537.30(32)**	**0.093(19)**	**0.00346**	($M1$)	
6669.02(16)	$1/2^+$	1440.11(15)	$(5/2^+)$	(5230.6(10))[h]	0.105(23)		[$E2$]	
		1188.38(14)	$3/2^-$	5481.17(95)[i]	0.036(14)		[$E1$]	
		726.56(5)	$3/2^-$	5942.8(13)[i]	0.024(14)		[$E1$]	
		529.56(10)	$3/2^-$	6139.60(34)	0.304(41)		[$E1$]	
		457.95(9)	$1/2^-$	6210.91(16)	0.243(19)		[$E1$]	
		450.23(11)	$3/2^-$	6218.64(31)	0.051(11)		[$E1$]	

involved, for a given PSF and LD model combination, the simulated physical quantities fluctuate between each capture-state decay simulation. The statistical variation of the decay provides an estimate of the uncertainty that may be attributed to the expected fluctuation properties of the simulated quantities. In this work we performed 50 separate nuclear realizations each comprising 100,000 capture-state decays to provide good statistical variation in the simulated level feedings.

IV. RESULTS AND DISCUSSION

Partial γ-ray production cross sections for 113 secondary γ rays and six newly-identified primary γ rays associated with the decay of 35 levels were obtained in the ^{180}W(n,γ) reaction and are listed in Table II. Together with this analysis, the placement of transitions in the ^{181}W decay scheme was accomplished using previous previous information from ENSDF [59]. Owing to the complexity of the singles capture-γ spectrum, several expected γ rays often contribute to a much larger multiplet. Accordingly, their corresponding intensities could only be resolved using ENSDF-reported branching ratios, or estimated based on statistical-model calculations. These transitions are identified in Table II. Of the 119 total reported γ rays, only 38 cross sections could be measured directly and the remainder were deduced indirectly as explained in Table II.

Because ^{180}W has a $J^\pi = 0^+$ ground state, the s-wave neutron-capture state populated in ^{181}W is a $J^\pi = 1/2^+$ state. Direct population of low-spin negative-parity excited states dominate the decay process. However, a broad spin window up to $J = 11/2\ \hbar$, via direct and indirect population of both positive- and negative-parity states, is observed. Where available, spins and parities of levels as well as transition multipolarities and mixing ratios (δ_γ) reported in Table II were taken from ENSDF [59]; spins and parities could be verified from the present analysis up to an excitation energy of 610 keV (the established $E_{\rm c}$, see Sect. IV A) by comparison with the corresponding level populations. Unknown multipolarities were assumed based on the lowest-order multipole consistent with angular momentum selection rules[a]. The level energies of ^{181}W in Table II were obtained from a least-squares fit to the E_γ data from the current measurement. These energies agree with the adopted energies in ENSDF [59] within uncertainties with the exception of S_n (see Sect. IV C). Presented internal conversion coefficients were recalculated with BRICC [43] based on the ENSDF information regarding transition multipolarities; our values generally compare well with the adopted dataset in ENSDF [59]. In the following discussion we describe how the experimental data obtained from ^{180}W(n,γ) measurement are used to evaluate the ^{181}W decay scheme, deduce σ_0, and provide a new precise determination of S_n for ^{181}W.

[a] In reality, many of these transitions are likely to have mixed-multipole character. For transitions with $E_\gamma \gtrsim 200$ keV this will have a negligible impact on α-corrected intensities; for transitions deexciting levels below $E_{\rm c}$, δ_γ could be adjusted to optimize agreement with statistical-model calculations.

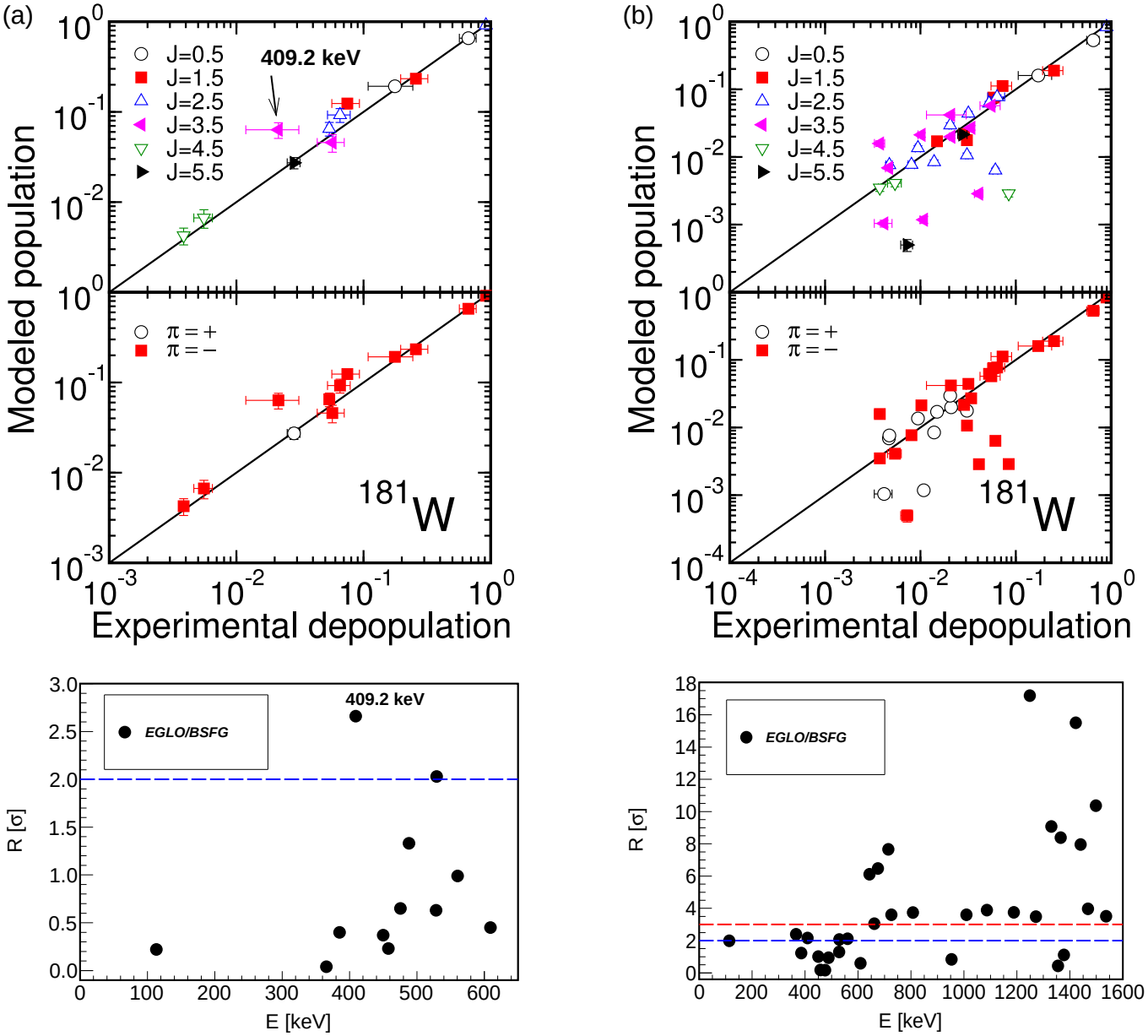

FIG. 2: (Color online) The simulated population per neutron capture ($P_i^{\rm sim}$, calculated with DICEBOX) versus the experimental depopulation per neutron capture ($P_i^{\rm exp}$, Eq. 5) to low-lying levels in ^{181}W. The EGLO/BSFG models (assuming the LD parametrization of Ref. [47, 48]) were adopted in the DICEBOX simulations. The spin distribution of low-lying levels is presented in the upper panel, and the parity distribution for the same plot is shown in the lower panel. The corresponding statistical significance of the residuals (R) between simulation and experiment for each population-depopulation plot are shown for all low-lying levels below $E_{\rm c}$: (a) $E_{\rm c} = 610$ keV; (b) $E_{\rm c} = 1538$ keV. A blue-dashed line is drawn at $R = 2\sigma$ in each of the residuals plots, and a red-dashed line at $R = 3\sigma$ is also shown in (b). Good agreement between experiment and simulation ($R < 3\sigma$) for all low-lying levels is shown in (a) where $E_{\rm c} = 610$ keV. Notably poorer agreement is observed in (b) assuming a much higher cut-off energy of 1538 keV. See text for details.

A. Constraints on ^{181}W decay scheme

It has been shown in our previous works on medium-mass [37, 40] and heavy nuclei [20] that comparison of experimental depopulation with simulated population of individual levels can be used for investigating the spins and parities, as well as completeness of the decay scheme, of the low-lying levels. The experimental intensities are determined in absolute cross sections while the simulated population $P_L^{\rm sim}$ as a fraction per neutron capture. Clearly, the two quantities must be presented with the same dimensions for meaningful comparison. Therefore, we converted experimental depopulation to intensity per

TABLE III: Total radiative thermal neutron-capture cross sections and simulated fraction of transitions to the ground state (σ_0 and P_0, respectively) and the $5/2^-$ metastable isomer at 365.6 keV ($\sigma_{5/2^-}$ and $P_{5/2^-}$, respectively) from levels above $E_c = 610$ keV. The mean s-wave capture-state radiative widths (Γ_0) for ^{180}W(n,γ) corresponding to various combinations of $E1$ PSF and LD models (acronyms are explained in the text) are listed in the final column. Experimentally-measured cross sections from levels below E_c are $\sum_{i=1}^{4} \sigma^{exp}_{\gamma_{i0}}(1+\alpha_{i0}) = 20.23(54)$ b for the ground state, and $\sum_{i=1}^{6} \sigma^{exp}_{\gamma_{i5/2^-}}(1+\alpha_{i5/2^-}) = 17.4(23)$ b for the isomer.

PSF/LD	P_0	σ_0 (b)	$P_{5/2^-}$	$\sigma_{5/2^-}$ (b)	Γ_0 [meV]
EGLO/BSFG[a]	0.071(21)	21.77(76)	0.138(26)	20.2(27)	86.7(28)
EGLO/BSFG[b]	0.057(21)	21.46(75)	0.143(30)	20.3(27)	85.4(25)
EGLO/CTF[a]	0.062(21)	21.58(75)	0.155(34)	20.6(28)	47.6(19)
EGLO/CTF[b]	0.050(21)	21.29(74)	0.141(27)	20.3(27)	41.4(21)
GLO/BSFG[a]	0.088(23)	22.18(82)	0.136(24)	20.2(27)	47.0(11)
GLO/BSFG[b]	0.071(23)	21.78(80)	0.141(28)	20.3(27)	46.6(10)
GLO/CTF[a]	0.077(23)	21.91(80)	0.151(31)	20.5(28)	26.2(7)
GLO/CTF[b]	0.062(23)	21.57(78)	0.140(24)	20.3(27)	23.2(7)
KMF/BSFG[a]	0.078(21)	21.94(78)	0.139(26)	20.2(27)	57.0(16)
KMF/BSFG[b]	0.064(21)	21.61(76)	0.145(29)	20.4(27)	55.6(14)
KMF/CTF[a]	0.068(21)	21.71(77)	0.155(33)	20.6(28)	31.4(10)
KMF/CTF[b]	0.055(22)	21.42(76)	0.142(26)	20.3(27)	27.2(11)
BA/BSFG[a]	0.036(15)	20.99(65)	0.155(35)	20.6(28)	157.4(54)
BA/BSFG[b]	0.031(14)	20.87(63)	0.160(39)	20.7(28)	148.3(48)
BA/CTF[a]	0.032(16)	20.89(66)	0.177(44)	21.2(30)	84.5(35)
BA/CTF[b]	0.027(17)	20.80(67)	0.156(37)	20.7(28)	69.6(36)

[a]Assuming the LD parametrization described in Ref. [47, 48].
[b]Assuming the LD parametrization described in Ref. [49].

neutron capture P_L^{exp} using the following relation

$$P_L^{exp} = \sum_{i=1}^{n} \frac{\sigma_{\gamma_i}(1+\alpha_i)}{\sigma_0}, \quad (5)$$

where n denotes the number of γ rays depopulating the level. The comparison of simulated population with experimental depopulation is shown in Fig. 2 for the EGLO/BSFG model combination, assuming the LD parametrization from Ref. [47, 48]. Uncertainties in the population along the vertical axis correspond to Porter-Thomas fluctuations from independent nuclear realizations, while those along the horizontal axis are attributable to the experimental uncertainty in the measured cross sections depopulating the levels. No error due to the uncertainty in σ_0 was assumed because this was only applied to normalize P_L^{exp}.

According to the present (n,γ) analysis and previous information in ENSDF we have determined $E_c = 610$ keV. In total, there are 16 known levels beneath 610 keV. Figure 2(a) shows the population-depopulation plot, together with the corresponding residuals, for the 13 levels we observed beneath E_c. The residuals show good agreement between simulations and experiment up to E_c, indicating that at least the part of the decay scheme relevant for thermal neutron capture is complete at these energies. The worst agreement corresponds to population of the 409.2-keV level; however, experiment and simulation still agree to within 3σ as revealed through the residuals. This level of agreement could be significantly improved by adjusting the mixing ratio of the 43.5-keV mixed $M1 + E2$ γ-ray transition. The *optimum* agreement would be obtained for $\delta_\gamma = 0.47$ but this would be at variance with the reported value of 0.10(3) [59], and correspond to increasing the $E2$ admixture from $\sim 1\%$ to 18%. Three additional levels at 250.7 ($J^\pi = 13/2^+$), 414.3 ($J^\pi = 15/2^+$), and 599.4 keV ($J^\pi = 13/2^+$), are also reported in ENSDF [59] that were not observed in the present measurement, nor expected to be populated in thermal neutron capture, because they represent part of a rotational sequence of very high spin levels with respect to the capture state $J^\pi = 1/2^+$. Consideration of these levels has no statistical influence on the results presented; similar findings were also reported in earlier work carried out on the major tungsten isotopes [20].

Four transitions deexciting levels below E_c could not

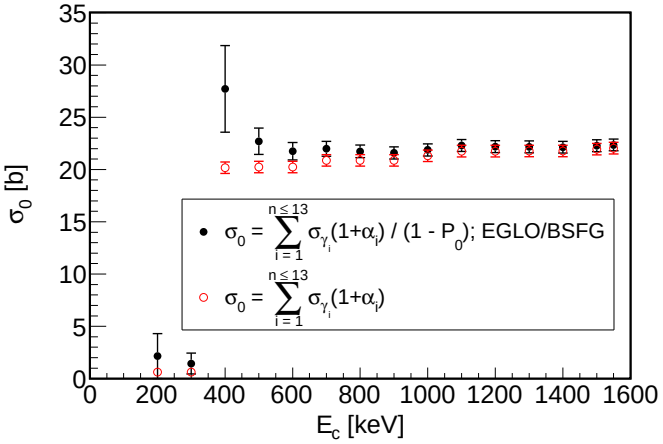

FIG. 3: (Color online) Variation of the total radiative thermal neutron-capture cross section (σ_0) with increasing cutoff energy, E_c, for the ^{180}W(n,γ) reaction. The red data points correspond to the determination of σ_0 by summing individual σ_γ contributions to the ground state. The total number of transitions observed feeding the ground state, n, is 13 when $E_c = 1550$ keV. The black data points also use the value of P_0 from DICEBOX calculations assuming the EGLO/BSFG model combination in the determination of σ_0 as a function of E_c. Very similar results are obtained with different PSF/LD combinations.

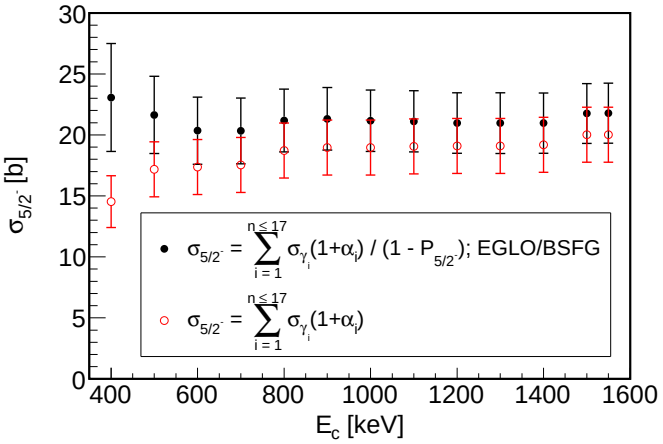

FIG. 4: (Color online) Variation of the radiative thermal neutron-capture cross section for the $J^\pi = 5/2^-$ metastable isomer ($\sigma_{5/2^-}$) with increasing cutoff energy, E_c, for the ^{180}W(n,γ) reaction. The red data points correspond to the determination of $\sigma_{5/2^-}$ by summing individual σ_γ contributions populating the 365.6-keV isomer. The total number of transitions observed feeding the isomer, n, is 17 when $E_c = 1550$ keV. The black data points also use the value of $P_{5/2^-}$ from DICEBOX calculations assuming the EGLO/BSFG model combination. Very similar results are obtained with different PSF/LD combinations. These cross-section data represent isomeric-feeding mechanisms and may be compared to the more precise measurement of $\sigma_{5/2^-} = 19.96(55)$ b deduced from its decay.

be resolved from their respective multiplets and were estimated from statistical-model calculations: 65.0 keV from the $3/2^-$ 450.2-keV level; 72.68 keV from the $1/2^-$ 458.0-keV level; and 133.7 and 243.5 keV, both from the $9/2^-$ 609.1-keV. An additional low-energy 19.7-keV transition deexciting the $1/2^-$ 385.3-keV level is beneath the HPGe-detection threshold and is also estimated based on statistical-model calculations. The predicted cross sections are indicated accordingly in Table II.

Beyond $E_c = 610$ keV, a new γ-ray transition at 349.06 keV is reported to deexcite the $7/2^-$ 714.6-keV level. This transition is assigned based on energy sums, after cross-checking against possible contaminant lines with similar energy, and is the first γ line observed from this level. A coincidence measurement, however, would ideally be needed to confirm its placement in the decay scheme. As illustrated in Fig. 2(b), increasing the decay-scheme cutoff energy above our established critical energy results in notably poorer agreement between simulation and experiment. Here, we set the cutoff energy to $E_c = 1538$ keV, the highest known level in ^{181}W [59] that can be populated by thermal neutron capture. No new levels were placed above this energy. For many transitions reported in this work, the complexity of the spectrum required use of ENSDF branching ratios to normalize weaker transitions to stronger γ rays, as indicated in Table II. The scatter of the data at $E_c = 1538$ keV in Fig. 2(b) indicates problems either with spins and parities of levels in this region, or with the completeness (γ rays and levels) of the decay scheme above $E_c = 610$ keV.

B. Radiative thermal neutron-capture cross section for ^{180}W(n,γ)

The total-capture cross section, σ_0, has been investigated for several combinations of PSF/LD models. This quantity is obtained using Eq. 3 assuming that the sum in the numerator corresponds to all transitions from levels below E_c and P_0 is the fractional contribution from all levels above E_c in the quasi continuum. Our results, presented in Table III, largely imply model independence. The experimentally-measured cross sections for transitions to the ground state from low-lying levels dominate the overall value of σ_0, with the largest contribution by far coming from the $5/2^- \rightarrow 9/2^+$ $M2$ transition at $E_\gamma = 365.6$-keV shown in Fig. 1 ($\sigma_\gamma = 19.55(54)$ b after correcting for conversion). The fraction P_0 is small even if the cutoff energy is raised above $E_c = 610$ keV, with the derived σ_0 remaining relatively constant. This stability is reflected in Fig. 3 where the cross section assuming the EGLO/BSFG model combination (using the LD parametrization from Ref. [47, 48]) is presented; here σ_0 is determined using P_0 calculated at the corresponding value of E_c. The statistically-insignificant dependence of σ_0 on E_c and PSF/LD model combination was also demonstrated in earlier work carried out on tungsten [20].

The EGLO, GLO, and KMF PSFs combined with BSFG and CTF LD models, and for each LD parametrization [47–49], all demonstrate reasonable

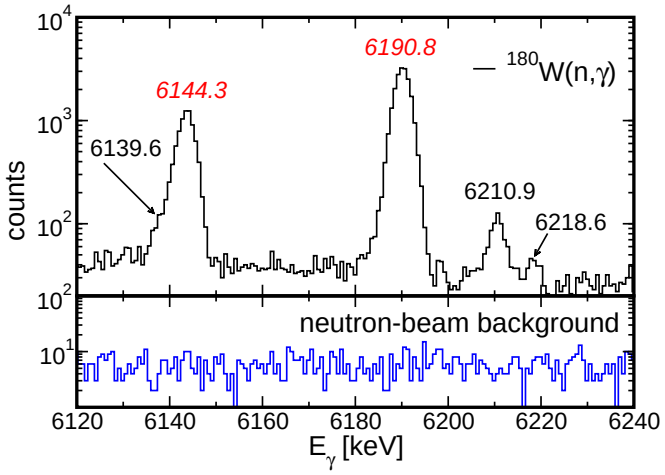

FIG. 5: (Color online) The black histograms in the upper panel shows the spectrum of primary γ rays belonging to ^{181}W following ^{180}W(n,γ); the blue histograms in the lower panel reveal a representative spectrum of the background produced by the neutron beam. Peaks from the ^{182}W(n,γ) reaction at 6144.3 and 6190.8 keV are also labeled. No background lines are observed in the regions of interest corresponding to ^{180}W(n,γ). The spectra are presented on a logarithmic scale to enhance weaker features.

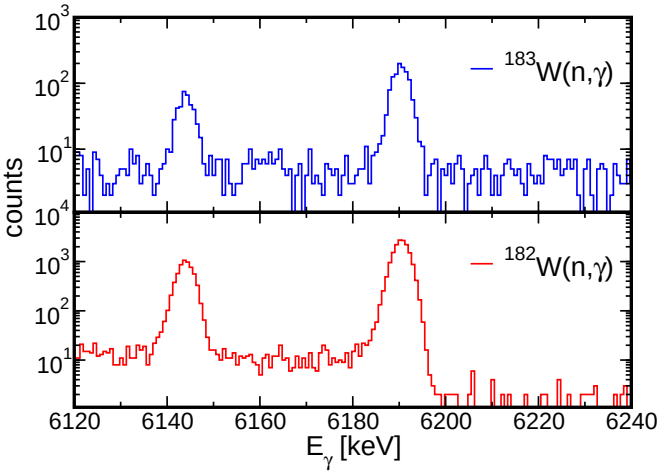

FIG. 6: (Color online) Spectra showing primary γ rays in the region around $E_\gamma = 6120 - 6240$ keV corresponding to (n,γ) measurements using samples of 92.7%-enriched ^{182}W (red histograms, lower panel), and 74.9%-enriched ^{183}W (blue histograms, upper panel) [20]. Only γ lines at 6144.3 and 6190.8 keV from ^{182}W(n,γ) are observed in this region; ^{182}W is present at the 9.0% level in the enriched ^{183}W sample [20]. There is no evidence for any transitions attributed to the ^{180}W(n,γ) reaction that would otherwise be observed in the displayed region. The spectra are presented on a logarithmic scale to enhance weaker features.

agreement in the determination of P_0 (Table III). A weighted average from these results yield $P_0 = 0.067(22)$, where the uncertainty represents the arithmetic mean of the individual associated uncertainties. Combining this P_0 with the experimental component comprising four direct ground-state feeding cross sections below E_c, i. e., $\sum_{i=1}^{4} \sigma_{\gamma_{i0}}(1+\alpha_{i0}) = 20.23(54)$ b, yields an adopted cross section $\sigma_0 = 21.67(77)$ b. Of the overall 3.56% uncertainty in our result, the statistical uncertainty dominates with a 2.69% contribution−which includes a systematic contribution from the normalization of the σ_γ data of $< 1.0\%$ folded quadratically. A contribution from the uncertainty in P_0 of 2.33% is also included. It should be noted that our adopted result compares very well with the value of σ_0 deduced from the sum of conversion-corrected measured cross sections corresponding to all 13 transitions that feed the ground state directly, indicated in bold in Table II, where $\sigma_0 = 22.04(55)$ b. Figure 3 also shows the experimental contribution alone to σ_0 as a function of E_c. Again, these results quickly converge to a statistically-consistent value. Compared to previous works, our value for σ_0 is consistent with the original limit set by Pomerance, $\sigma_0 = 30^{+120}_{-30}$ b [4], and appears consistent with the activation measurement of Kang *et al.* where they deduced the cross section for ^{180}W(n,γ) relative to that of ^{184}W(n,γ) [60] and ^{186}W(n,γ) [61], to give a weighted result $\sigma_0 = 22.6(17)$ b [5]. However, if we substitute our recent σ_0 measurements for ^{184}W(n,γ) and ^{186}W(n,γ) together with our P_γ measurements from the decay of ^{187}W [20] for the corresponding quantities used in Ref. [5], adopting their procedure we find a weighted average $\sigma_0 = 19.5(16)$ b for ^{180}W(n,γ). These results still agree fairly well. Finally, our measurement diagrees with the work of Vorona *et al.*, $\sigma_0 = 37.3(24)$ b [6].

We also report a new measurement for the total cross section, $\sigma_{5/2^-}(^{181}\mathrm{W}^m)$, feeding the short-lived $5/2^-$-metastable 14.59(15)-μs isomer at 365.6 keV [59]. The cross section is most accurately determined by measuring the total depopulation cross section of the isomer, $\sigma_{5/2^-}(^{181}\mathrm{W}^m) = 19.96(55)$ b. This result may then be cross checked by appropriately adapting Eq. 3 for $\sigma_{\gamma_{i5/2^-}}$, $\alpha_{i5/2^-}$ and $P_{5/2^-}$, where we find $\sum_{i=1}^{6} \sigma_{\gamma_{i5/2^-}}(1+\alpha_{i5/2^-}) = 17.4(23)$ b for the six direct isomer-feeding transitions below E_c and, using the same arguments for determining P_0 earlier, we report a corresponding average $P_{5/2^-} = 0.143(28)$ to give $\sigma_{5/2^-}(^{181}\mathrm{W}^m) = 20.3(27)$ b, consistent with the measured depopulation. This result is also consistent with the determination of the cross section from the summation of all 17 transitions (including those above E_c) italicized in Table II that feed the isomer directly, $\sigma_{5/2^-}(^{181}\mathrm{W}^m) = 20.0(23)$ b. The isomer cross section is plotted as a function of E_c in Fig. 4 assuming the EGLO/BSFG model combination with the LD parametrization of Ref. [47, 48]. The individual contribution to the isomer cross section from experimental feeding alone is also shown in Fig. 4. As with σ_0, we find $\sigma_{5/2^-}$ to converge quickly and is also largely independent of adopted model and E_c. Furthermore, because the cross sections for population of both the ground state (Fig. 3) and the 365.6-keV isomer (Fig. 4) become nearly

constant between $E_c = 610 - 1550$ keV renders any missing or unknown decay-scheme information insignificant.

Overall, our adopted results are best described using the EGLO/BSFG model combination. This selection is motivated by consideration to the residuals between experiment and simulation (Fig. 2(a)), and also reproduction of the mean total capture-state radiative width, Γ_0. Table III reveals Γ_0 is highly sensitive to the adopted model combination. Although model combinations invoking the KMF and GLO models also satisfy the first criterion fairly well, the EGLO/BSFG combination also reasonably reproduces the experimental width $\Gamma_0 = 70(10)$ meV [62]. The BA model is ruled out owing to poorer agreement between experimental and simulated populations (particularly for high-J states); similar observations have been encountered with the BA model in earlier works, e.g., see Refs. [20, 37, 63, 64].

C. Neutron-separation energy for ^{181}W

Analysis of primary γ rays using the PGAA method has already been successfully demonstrated to provide independent information on the neutron-separation energy S_n if both primary and secondary transitions are observed [20, 39]. In the present study, primary γ rays were identified for the first time from the ^{180}W(n,γ) reaction, permitting the most accurate determination of S_n in ^{181}W.

The recommended value from the AME2012 Atomic Mass Evaluation is 6686(5) keV [7]. But no primary γ rays connecting the capture state at this energy to low-lying levels with $J = 1/2$ or $3/2$ could be identified in our experiment, even at 3σ. However, despite the complexity of the γ-ray spectrum due to the presence of several isotopes, we are nevertheless able to identify all observed γ lines with $E_\gamma \gtrsim 5$ MeV (see Fig. 1). The only transitions that could not be assigned to other tungsten isotopes (or background) at these energies are those assigned to the decay of the capture state in Table II which perfectly fit to $S_n = 6669.02(16)$ keV. All assigned transitions (excluding the tentatively placed 5230.6-keV γ ray in Table II) are of $E1$ character. In accordance with angular momentum selection rules, a primary γ-ray transition is not expected to feed the ground state in ^{181}W; this inference is reinforced by the notable lack of any peak at the deduced position of S_n in the observed γ-ray spectrum presented in the lower panel of Fig. 1.

A spectrum of γ rays expanded around the principal region of observed ^{180}W(n,γ) primaries is shown in Fig. 5. The background at the PGAA facility is very well understood [23, 65], both with *beam on* and *beam off*, thereby preventing false-positive identification through background signals. A representative beam-on background spectrum is also shown in Fig. 5 and is clearly void of any transitions in the region of interest pertaining to candidate ^{180}W(n,γ) primaries. We also present in Fig. 6 spectra measured at the same facility for 92.7% and 74.9% enriched ^{182}W and ^{183}W targets [20]. Only transitions from thermal neutron capture on these two isotopes contribute at $E_\gamma > 5.8$ MeV; S_n values of the other contaminant tungsten isotopes produced in the enriched-^{180}W sample are lower with $S_n = 5753.7$ and $S_n = 5466.6$ keV for ^{185}W and ^{187}W, respectively [20]. Only γ lines at 6144.3 and 6190.8 keV from ^{182}W(n,γ) are observed in this region of the spectra for contaminants; there was a 9.0% contamination of ^{182}W in the enriched ^{183}W sample [20]. These observations manifestly establish that the new γ lines at 6210.9 and 6218.5 keV in Fig 5 can only be attributed to the ^{180}W(n,γ) reaction. The transition at 6139.6 keV sits on the low-energy shoulder of the much stronger 6144.3-keV ^{182}W(n,γ) primary. An analysis of the residuals between fitted lineshape and observed counts clearly demonstrated the presence of a doublet in the ^{180}W(n,γ) spectrum. However, the same region is well fitted as a singlet transition in both the ^{182}W(n,γ) and ^{183}W(n,γ) spectra. Possible escape peaks were also ruled out in validating ^{180}W(n,γ) primary γ-ray assignments.

Weaker $E1$ transitions at 5481.2 keV and 5942.8 keV (Table II) are observed in the ^{180}W(n,γ) spectrum and assigned as primary transitions in ^{181}W. A transition is also oberved at 5230.6 keV in Fig. 1. This transition cannot be identified with any known activity from other tungsten or trace isotopes present in the sample, nor does it correspond to the known background. A possible placement feeding the 1440.1-keV level would imply it must have $E2$ character and thus, constrain the spin-parity of the 1440.1-keV level to $J^\pi = 5/2^+$. The cross section of this transition is unusually large for an $E2$ although it is consistent with the intensity balance of the level. After further cross checking against the Evaluated Gamma-ray Activation File (EGAF) database [66, 67], it appears likely that this is a primary γ ray in ^{181}W although we consider it a tentative assignment at this time and do not include it in the preceeding statistical analysis. The proposed value of S_n is obtained from a global fit to the γ-ray data in Table II, whereupon consideration for the expression

$$S_n = E_\gamma + E_f + E_r, \tag{6}$$

for the three strongest primary $E1$ transitions, is used to determine the mean-reported value. Here, $E_r = E_\gamma^2/2A$ is the nuclear-recoil energy and E_γ is in units of MeV. The overall uncertainty in our result, $S_n = 6669.02(16)$ keV, represents an order of magnitude improvement in resolution over the previously adopted value [7].

V. CONCLUSION

For the first time, a set of partial γ-ray production cross sections has been measured from the ^{180}W(n,γ) reaction using thermal neutrons. These cross sections

are combined with DICEBOX statistical-model simulations to yield the total radiative thermal neutron-capture cross section, $\sigma_0 = 21.67(77)$ b, as well as the total cross section for the 365.6-keV $5/2^-$ metastable isomer, $\sigma_{5/2^-}(^{181}\mathrm{W}^m,\ 14.6\ \mu\mathrm{s}) = 19.96(55)$ b. Our result for σ_0 compares well with a previous activation measurement, reported in Ref. [5] as $\sigma_0 = 22.6(17)$ b and lowered slightly to $\sigma_0 = 19.5(16)$ b after renormalization with our σ_0 and P_γ results from Ref. [20], but disagrees by more than six standard deviations with the work of Vorona *et al.*, $\sigma_0 = 37.3(24)$ b [6]. It was found that the total cross section is (almost) insensitive to adopted models of photon strength functions and level densities used in the simulations. Far greater sensitivity, however, is observed in the determination of the mean total capture-state width. Although Γ_0 values generated using the EGLO/BSFG, KMF/BSFG, and BA/CTF combinations all compare fairly well with the adopted width, $\Gamma_0 = 70(10)$ meV [62], the EGLO/BSFG is our preferred choice owing to superior residuals between simulated population and measured depopulation data up to a recommended critical energy, $E_\mathrm{c} = 610$ keV. Our established value of E_c suggests the level scheme for ^{181}W is complete and accurate up to this excitation energy and may serve as a useful guide for Hauser-Feshbach practitioners.

Identification of several primary γ rays from the $^{180}\mathrm{W}(n,\gamma)$ reaction allowed us to determine the neutron-separation energy in ^{181}W to a high level of precision, $S_n = 6669.02(16)$ keV. This result represents an order of magnitude improvement in uncertainty over the currently adopted value [7] which we also disagree with by more than three standard deviations. Our improved reaction cross-section and separation-energy results provide useful augmentation for the neutron data libraries and atomic mass evaluations, respectively.

Acknowledgments

This work was performed under the auspices of the University of California, supported by the Director, Office of Science, Office of Basic Energy Sciences, of the U. S. Department of Energy at Lawrence Berkeley National Laboratory under Contract DE-AC02-05CH11231, the U. S. Department of Energy by Lawrence Livermore National Laboratory under Contract DE-AC52-07NA27344. Access to the Budapest PGAA facility was supported by the NAP VENEUS08 grant under Contract OMFB-00184/2006. This work was also supported by the Czech Science Foundation under Grant No. 13-07117S. The operations staff at the Budapest Research Reactor are gratefully acknowledged. One of the authors (AH) would like to thank Dr. R. D. Hoffman for reviewing the manuscript.

[1] M. Berglund and M. Wiesser, Pure Appl. Chem. **83**, 397 (2011).
[2] S. E. Woosley and W. M. Howard, Astrophys. J. Suppl. **36**, 85 (1978).
[3] T. Rauscher, A. Heger, R. D. Hoffman, and S. E. Woosley, Astrophys. J. **576**, 323 (2002).
[4] H. Pomerance, Phys. Rev. **88**, 412 (1952).
[5] W. G. Kang et al., Phys. Rev. C **76**, 067602 (2007).
[6] P. N. Vorona, O. I. Kalchenko, and V. G. Krivenko (Kyiv, Ukraine, 2008), Second Int. Conf. Cur. Prob. in Nucl. Phys. Atom. Ene., p. 528.
[7] M. Wang et al., Chin. Phys. C **16**, 1603 (2012).
[8] M. Chadwick et al., Nucl. Data Sheets **112**, 2887 (2011), URL `http://www-nds.iaea.org/exfor/endf.htm/`.
[9] R. Capote et al., Nucl. Data Sheets **110**, 3107 (2009), URL `http://www-nds.iaea.org/RIPL-3/`.
[10] I. E. Peterson and R. E. Miller, Russian J. Ecol. **39**, 495 (2008).
[11] T. Sotobayashi, T. Suzuki, and T. Noda, Bull. Chem. Soc. Japan **43**, 3005 (1970).
[12] B. V. Kurchatov, V. N. Lavrenchik, and V. M. Shubko, Atomnaya Energiya **13**, 1206 (1962).
[13] N. P. Dikiy et al., Prob. Atom. Sci. Tech. **36**, 58 (2000).
[14] S. Jednorog et al., J. Radioanal. Nucl. Chem. **303**, 1009 (2015).
[15] J. S. E. Wieslander et al., Nucl. Instrum. Methods Phys. Res. Sect. A **591**, 383 (2008).
[16] A. Kumar et al., Fusion Tech. **19**, 1859 (1991).
[17] H. Y. Khater and M. E. Sawan (Alburquerque, New Mexico, 1999), 18th IEEE/NPSS Symposium on Fusion Engineering, p. 475.
[18] P. Anselmann et al., Phys. Letts. B **342**, 440 (1995), (GALLEX Collaboration).
[19] J. N. Abdurashitov et al., Phys. Rev. Lett. **77**, 4708 (1996).
[20] A. M. Hurst et al., Phys. Rev. C **89**, 014606 (2014).
[21] T. Belgya et al. (Springer Verlag, Budapest, Hungary, 1997), Proc. 9th International Symposium on Capture Gamma-Ray Spectroscopy and Related Topics, p. 826.
[22] L. Rosta, Appl. Phys. A **74**, S52 (2002).
[23] Zs. Révay et al., Nucl. Instrum. Methods Phys. Res. Sect. B **213**, 385 (2004).
[24] L. Szentmiklósi et al., J. Radioanal. Nucl. Chem. **286**, 501 (2010).
[25] R. M. Lindstrom and Zs. Révay, *Handbook of Prompt Gamma Activation Analysis*, chap. Beams and Facilities, p. 31, in [68] (2004).
[26] T. Belgya, Phys. Proc. **31**, 99 (2012).
[27] T. Belgya, Z. Kis, and L. Szentmiklósi, Nucl. Data Sheets **119**, 419 (2014).
[28] T. Belgya and L. Szentmiklósi, Private communication.
[29] B. Fazekas et al., J. Radioanal Nucl. Chem. **215**, 271 (1997).
[30] Zs. Révay, T. Belgya, P. P. Ember, and G. L. Molnár, J. Radioanal. Nucl. Chem. **248**, 401 (2001).
[31] G. Molnár, Zs. Révay, and T. Belgya, Nucl. Instrum. Methods Phys. Res. Sect. A **489**, 140 (2002).
[32] *Hypermet-PC Version 5.01 (v512)* (1995-97), Institute

of Isotopes, Budapest, Hungary, URL http://www.iki.kfki.hu/nuclear/hypc/.
[33] Zs. Révay and G. L. Molnár, Radiochim. Acta **91**, 361 (2003).
[34] Z. Kis et al., Nucl. Instrum. and Methods Phys. Res. Sect A **418**, 374 (1998).
[35] Zs. Révay, Anal. Chem. **81**, 6851 (2009).
[36] G. L. Molnár, Zs. Révay, and T. Belgya, Nucl. Instrum. and Methods Phys. Res. Sect. B **213**, 32 (2004).
[37] M. Krtička et al., Phys. Rev. C **77**, 054615 (2008).
[38] R. B. Firestone, M. Krtička, Zs. Révay, L. Szentmiklósi, and T. Belgya, Phys. Rev. C **87**, 024605 (2013).
[39] R. B. Firestone, Zs. Révay, and T. Belgya, Phys. Rev. C **89**, 014617 (2014).
[40] H. D. Choi et al., Nucl. Sci. Eng. **177**, 219 (2014).
[41] F. Bečvář, Nucl. Instrum. Methods Phys. Res. Sect. A **417**, 434 (1998).
[42] N. Bohr, Nature (London) **137**, 344 (1936).
[43] T. Kibédi et al., Nucl. Instrum. Methods Phys. Res. Sect. A **589**, 202 (2008).
[44] C. E. Porter and R. G.Thomas, Phys. Rev. **104**, 483 (1956).
[45] A. G. Gilbert and A. G. Cameron, Can. J. Phys. **43**, 1446 (1965).
[46] T. D. Newton, Can. J. Phys. **34**, 804 (1956).
[47] T. von Egidy and D. Bucurescu, Phys. Rev. C **72**, 044311 (2005).
[48] T. von Egidy and D. Bucurescu, Phys. Rev. C **73**, 049901(E) (2006).
[49] T. von Egidy and D. Bucurescu, Phys. Rev. C **80**, 054310 (2009).
[50] S. I. Al-Quraishi, S. M. Grimes, T. N. Massey, and D. A. Resler, Phys. Rev. C **67**, 015803 (2003).
[51] D. M. Brink, Ph.D. thesis, University of Oxford (1955).
[52] P. Axel, Phys. Rev. **126**, 671 (1962).
[53] S. G. Kadmenski, V. P. Markushev, and V. I. Furman, Yad. Fiz. **37**, 277 (1983), [Sov. J. Nucl. Phys. **37**, 165 (1983)].
[54] J. Kopecky and M. Uhl, Phys. Rev. C **41**, 1941 (1990).
[55] J. Kopecky, M. Uhl, and R. E. Chrien, Phys. Rev. C **47**, 312 (1993).
[56] G. A. Bartholomew, Ann. Rev. Nucl. Sci. **11**, 275 (1961).
[57] J. Speth and A. van der Woude, Rep. Prog. Phys. **44**, 719 (1981).
[58] W. V. Prestwitch, M. A. Islam, and T. J. Kennett, Z. Phys. A **315**, 103 (1984).
[59] S. C. Wu, Nucl. Data Sheets **106**, 367 (2005).
[60] V. Bondarenko et al., Nucl. Phys. **A762**, 167 (2005).
[61] M. Karadag et al., Ann. Nucl. Energy **31**, 1285 (2004).
[62] S. F. Muhghabghab, *Atlas of Neutron Resonances: Resonance Parameters and Thermal Cross Sections Z = 1-100* (Elsevier BV, New York, 2006), 5th ed.
[63] M. Guttormsen et al., Phys. Rev. C **71**, 044307 (2005).
[64] A. C. Larsen et al., Phys. Rev. Lett. **111**, 242504 (2013).
[65] T. Belgya, Zs. Révay, and G. L. Molnár, J. Radioanal. Nucl. Chem. **265**, 181 (2005).
[66] Zs. Révay, R. B. Firestone, T. Belgya, and G. L. Molnár, *Handbook of Prompt Gamma Activation Analysis*, chap. Prompt Gamma-Ray Spectrum Catalog, p. 173, in [68] (2004).
[67] R. B. Firestone, *Database of Prompt Gamma Rays from Slow Neutron Capture for Elemental Analysis* (International Atomic Energy Agency, Vienna, 2006), chap. Adopted Database and User Tables, p. 73, URL http://www-nds.iaea.org/pgaa/egaf.html.
[68] G. L. Molnár, ed., *Handbook of Prompt Gamma Activation Analysis* (Kluwer Academic Publishers, The Netherlands, 2004).